

# Laplacian Spectral Distances and Kernels on 3D Shapes

Giuseppe Patané<sup>a</sup>

<sup>a</sup>Consiglio Nazionale delle Ricerche  
Istituto di Matematica Applicata e Tecnologie Informatiche  
Via De Marini, 6, 16149 Genova, Italy  
patane@ge.imati.cnr.it

---

## Abstract

This paper presents an alternative means of deriving and discretizing spectral distances and kernels on a 3D shape by filtering its Laplacian spectrum. Through the selection of a filter map, we design new spectral kernels and distances, whose smoothness and encoding of both local and global properties depend on the convergence of the filtered Laplacian eigenvalues to zero. Approximating the discrete spectral distances through the Taylor approximation of the filter map, the proposed computation is independent of the evaluation of the Laplacian spectrum, bypasses the computational and storage limits of previous work, which requires the selection of a specific subset of eigenpairs, and guarantees a higher approximation accuracy and a lower computational cost.

**Keywords:** Spectral distances, Biharmonic and diffusion distances, Laplace-Beltrami operator, Shape analysis, Discrete geometry, Laplacian matrix.

---

## 1. Introduction

In geometry processing and shape analysis, several problems have been addressed through the properties of the heat diffusion kernel on a 3D shape, such as shape segmentation [13] and comparison [9, 7, 15, 17, 26] through heat kernel shape descriptors [32] and auto-diffusion maps [17]. The Laplacian spectrum is also fundamental to define random walks [31], commute-time [8], biharmonic [25, 33], wave kernel [8, 2], and diffusion distances [6, 7, 11, 17, 21, 38, 29]. Further applications include dimensionality reduction [3, 39] with spectral embeddings, the computation of the gradient of discrete maps [38], and the multi-scale approximation of functions [27, 28].

This growing interest on the biharmonic, heat diffusion, and wave kernel distances is motivated by their capability of encoding local geometric properties (e.g., Gaussian curvature, geodesic distance) of the input shape. Additional properties, such as the intrinsic and multi-scale definition with respect to the input shape, the invariance to isometries, the shape-awareness, the robustness to noise and tessellation, make these distances particularly suitable to address several applications in shape analysis, segmentation, and matching.

Starting from recent work [12, 27], which has been focused on the computation of the geodesic and heat diffusion distances, we address the definition and computation of spectral distances on a manifold  $\mathcal{M}$  (Sect. 2). As *spectral distance*  $d^2(\mathbf{p}, \mathbf{q}) := \sum_{n=0}^{+\infty} \varphi^2(\lambda_n) |\phi_n(\mathbf{p}) - \phi_n(\mathbf{q})|^2$ , we refer to any distance on  $\mathcal{M}$  that can be defined through a filtering  $(\varphi(\lambda_n))_{n=0}^{+\infty}$  of the Laplacian spectrum  $\{(\lambda_n, \phi_n)\}_{n=0}^{+\infty}$  of  $\mathcal{M}$ . Here,  $\varphi: \mathbb{R}^+ \rightarrow \mathbb{R}$  is a strictly positive and square integrable map. In particular, the corresponding *spectral kernel*  $K(\cdot, \cdot)$  is defined as the map that verifies the relation

$$d(\mathbf{p}, \mathbf{q}) = \|K(\mathbf{p}, \cdot) - K(\mathbf{q}, \cdot)\|_2.$$

Different filter maps identify spectral distances introduced by previous work. For *poly-harmonic distances* induced by  $\varphi(s) := s^{-k/2}$ , the larger Laplacian eigenvalues are enhanced by selecting a low degree  $k$ . *Mexican hat wavelets* [20] are generated by the filter  $\varphi(s) := s^{1/2} \exp(-s^2)$  and in [8, 2] the map  $\varphi_t(s) := \exp(is)$ ,  $s \in [0, 2\pi]$ , defines the wave kernel signature. Similarly to random walks [31], we consider the filter map  $\varphi_t(s) = t^k s^\alpha \exp(-ts^\alpha)$ , where  $k$  scales the diffusion rate and  $\alpha$  controls the distance smoothness. The selection of the filter map allows us to adapt the corresponding spectral distances to specific features of the input data and characterize intrinsic shape properties. In this way, we provide a simple procedure to design new spectral kernels and distances, whose smoothness and encoding of both local and global properties depend on the convergence of the filtered Laplacian eigenvalues to zero. Increasing the filter decay to zero, the effects of larger eigenvalues and of the corresponding eigenvectors on the filtered spectral distance are negligible with respect to the contribution of the lower eigenvalues. The resulting distance encodes the global features of the input shape, while poorly identifying its local properties. Reducing the filter decay to zero, local shape features are better characterized.

Rewriting the Laplacian matrix as  $\tilde{\mathbf{L}} := \mathbf{B}^{-1}\mathbf{L}$ , where  $\mathbf{L}$  is a symmetric, positive semi-definite matrix and  $\mathbf{B}$  is symmetric and positive definite, we derive the discrete spectral kernel  $\mathbf{K} := \mathbf{X}\varphi(\Lambda)\mathbf{X}^\top\mathbf{B}$ ,  $\varphi(\Lambda) := \text{diag}(\varphi(\lambda_i))_{i=1}^n$ . Here,  $\mathbf{X}$  is the eigenvectors' matrix associated to the generalized eigenproblem  $\mathbf{L}\mathbf{X} = \mathbf{B}\mathbf{X}\Lambda$  and  $\Lambda := \text{diag}(\lambda_i)_{i=1}^n$ ,  $0 \leq \lambda_i \leq \lambda_{i+1}$ , is the eigenvalue matrix. For this representation, which holds for polygonal meshes and point sets, the orthogonality of the Laplacian eigenvectors with respect to the  $\mathbf{B}$ -scalar product

$\langle \mathbf{f}, \mathbf{g} \rangle_{\mathbf{B}} := \mathbf{f}^\top \mathbf{B} \mathbf{g}$  is crucial to encode the geometry of the surface underlying  $\mathcal{S}$  in the spectral kernel and makes its evaluation robust to surface sampling.

Our approximation (Sect. 3) is independent of the computation of the Laplacian spectrum, which is generally unfeasible in terms of memory storage and computational cost, even by applying iterative solvers of sparse eigenproblems with super linear time complexity [35]. Furthermore, it avoids the selection of a subset of Laplacian eigenpairs and the use of multiresolutive prolongation operators [37], which heuristically adapt the number of eigenpairs and/or the surface resolution to its global/local features. The novelty of our approach is to approximate any spectral distance using an  $r$ -degree Taylor polynomial approximation of the filter map. In this way, the spectral distances are computed through the solution of  $r$  sparse linear systems in  $O(rn)$  time with iterative solvers, such as the Jacobi, Gauss-Seidel, minimum residual methods [18], and without extracting the Laplacian spectrum. Since the proposed approximation scheme works mainly with matrices, the evaluation of the spectral distances is independent of the discretization of the input surface as a polygonal mesh or a point cloud.

For the heat diffusion distance, we also apply the  $(r, r)$ -degree Padé-Chebyshev rational polynomial approximation [10, 18, 24, 36] of the exponential map with respect to the  $\ell_\infty$  norm. In this case, the approximation accuracy of the heat diffusion distance is lower than  $10^{-r}$  and it can be further reduced by slightly increasing the degree  $r$  of the rational Padé-Chebyshev polynomial (e.g.,  $r := 5, 7$  in our experiments). The Padé-Chebyshev approximation has been applied to the wavelet operator for applications in spectral graph theory [19] but its use for the computation of the heat diffusion distance has not been addressed.

To speed-up the computation of the spectral distances among a large number of points, it is sufficient to apply iterative solvers of linear systems or a pre-factorization of the coefficient matrices. Our experiments (Sect. 4) show that the proposed algorithm is also robust with respect to irregular sampling density, noise, and mesh degeneracies; can be applied to different Laplacian weights; and is free of user-defined parameters. On the contrary (Sect. 5), in previous work the resolution of the simplified approximation of the input surface, on which the Laplacian matrix is computed, and the number of Laplacian eigenpairs are tuned according to the target approximation accuracy.

## 2. Laplacian spectral distances

The idea behind the proposed approach is to define the spectral kernels and the corresponding distances in the frequency domain (Sect. 2.1) through the filtering of the spectral decomposition of the Laplace-Beltrami operator (Sect. 2.2).

### 2.1. Spectral distances

Let  $\mathcal{L}_2(\mathcal{M})$  be the space of square integrable maps on a compact Riemannian manifold  $\mathcal{M}$ , endowed with the prod-

uct  $\langle f, g \rangle_2 := \int_{\mathcal{M}} f(\mathbf{p})g(\mathbf{p})\mu(d\mathbf{p})$ , where  $\mu$  is a (Borel) measure on  $\mathcal{M}$ . Let  $\varphi: \mathbb{R}^+ \rightarrow \mathbb{R}$  be a strictly positive and square integrable filter map and  $(\lambda_n, \phi_n)_{n=0}^{+\infty}$ ,  $\Delta\phi_n = \lambda_n\phi_n$ ,  $\lambda_n \leq \lambda_{n+1}$ , the Laplacian eigensystem. Considering the power series  $\varphi(s) = \sum_{n=0}^{+\infty} \alpha_n s^n$  and noting that  $\Delta^i f = \sum_{n=0}^{+\infty} \lambda_n^i \langle f, \phi_n \rangle_2 \phi_n$ , on  $\mathcal{L}_2(\mathcal{M})$  we define the spectral operator

$$\begin{aligned} \Phi(f) &= \sum_{n=0}^{+\infty} \alpha_n \Delta^n f = \sum_{n,m=0}^{+\infty} \alpha_n \lambda_n^n \langle f, \phi_m \rangle_2 \phi_m \\ &= \sum_{n=0}^{+\infty} \varphi(\lambda_n) \langle f, \phi_n \rangle_2 \phi_n. \end{aligned} \quad (1)$$

The linear operator  $\Phi$  is continuous ( $\|\Phi(f)\|_2 \leq \|\varphi\|_2 \|f\|_2$ ) and  $\Phi(f) = K \star f$ , where  $K(\mathbf{p}, \mathbf{q}) = \sum_{n=0}^{+\infty} \varphi(\lambda_n) \phi_n(\mathbf{p}) \phi_n(\mathbf{q})$  is the spectral kernel. Since

$$\|K(\cdot, \cdot)\|_2^2 = \sum_{n=0}^{+\infty} |\varphi(\lambda_n)|^2 \left[ \int_{\mathcal{M}} |\phi(\mathbf{p})|^2 \mu(d\mathbf{p}) \right] \leq \|\varphi\|_2^2.$$

the kernel is well-defined; the symmetry and self-adjointness of  $K(\cdot, \cdot)$  follow from its spectral representation. Through the spectral operator, in  $\mathcal{L}_2(\mathcal{M})$  we introduce the scalar product and the corresponding distance as

$$\begin{cases} \langle f, g \rangle := \langle \Phi(f), \Phi(g) \rangle_2 = \sum_{n=0}^{+\infty} \varphi^2(\lambda_n) \langle f, \phi_n \rangle_2 \langle g, \phi_n \rangle_2, & (a) \\ d^2(f, g) = \|f - g\|^2 = \sum_{n=0}^{+\infty} \varphi^2(\lambda_n) |\langle f - g, \phi_n \rangle_2|^2. & (b) \end{cases} \quad (2)$$

Indicating with  $\delta_{\mathbf{p}}$  the map that takes value 1 at  $\mathbf{p}$  and 0 otherwise, the spectral distance between  $\mathbf{p}, \mathbf{q}$  is

$$d^2(\mathbf{p}, \mathbf{q}) := \|\delta_{\mathbf{p}} - \delta_{\mathbf{q}}\|^2 = \sum_{n=0}^{+\infty} \varphi^2(\lambda_n) |\phi_n(\mathbf{p}) - \phi_n(\mathbf{q})|^2.$$

The distance  $d(\cdot, \cdot)$ , which is defined by filtering of the Laplacian eigensystem, is also expressed through the kernel as  $d(\mathbf{p}, \mathbf{q}) = \|K(\mathbf{p}, \cdot) - K(\mathbf{q}, \cdot)\|_2$ .

The space  $\mathcal{L}_2(\mathcal{M})$  is complete with respect to the norm induced by the spectral scalar product; i.e., given a Cauchy sequence  $(f_n)_{n=0}^{+\infty}$  in  $\mathcal{L}_2(\mathcal{M})$  there exists  $f \in \mathcal{L}_2(\mathcal{M})$  such that  $\lim_{n \rightarrow +\infty} \|f_n - f\| = 0$ . Since  $(f_n)_{n=0}^{+\infty}$  is a Cauchy sequence,  $\|f_n - f_m\|^2 = \sum_{k=0}^{+\infty} \varphi^2(\lambda_k) |\langle f_n - f_m, \phi_k \rangle_2|^2$  converges to zero and  $\lim_{n,m \rightarrow +\infty} |\langle f_n - f_m, \phi_k \rangle_2| = 0$ ,  $k \in \mathbb{N}$ . Indeed,  $(\langle f_n, \phi_k \rangle_2)_{n=0}^{+\infty}$  is a Cauchy sequence that converges to  $\alpha_k \in \mathbb{R}$ . Then, we define the map  $f = \sum_{n=0}^{+\infty} \alpha_n \phi_n$  and the norm  $\|f_n - f\| = \sum_{k=0}^{+\infty} \varphi^2(\lambda_k) |\langle f_n - f, \phi_k \rangle_2|^2$  converges to zero, thus showing the completeness of  $\mathcal{L}_2(\mathcal{M})$  with respect to (2a).

To estimate the stability of the spectral distance, we perturb the input map  $f: \mathcal{M} \rightarrow \mathbb{R}$  with a function  $e$  and notice that

$$|d^2(f, g + e) - d^2(f, g)| = \sum_{n=0}^{+\infty} \varphi^2(\lambda_n) |\langle e, \phi_n \rangle_2|^2 \leq \|\varphi\|_2^2 \|e\|_2^2;$$

i.e., the resulting variation on  $d(\cdot, \cdot)$  is bounded by  $\|\varphi\|_2 \|e\|_2$ . Without loss of generality, we normalize the filter as  $\varphi/\|\varphi\|_\infty$  and conclude that the variation of the spectral distance is proportional to the perturbation of the input map.

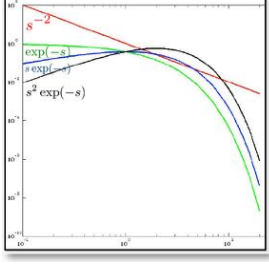


**Figure 1:** Spectral distances and kernels induced by the filter map  $\varphi$  (log-scale on the  $t$ - and  $y$ -axis) applied to the Laplacian eigenvalues.

## 2.2. Selection of the filter map

The filter map is chosen in such a way that both local and global properties of the input shape are encoded in the corresponding spectral distance. For instance (Fig. 1), selecting  $\varphi_t(s) := \exp(-s)$ ,  $\exp(-ist)$  or  $\varphi(s) := s^{-k/2}, s^{-1/2}$ , we get the *heat diffusion*, *wave*, or *poly-harmonic*, *commute-time distances*, respectively. On the one hand, the effects of the Laplacian eigenvalues of larger magnitude are enhanced by selecting a low degree  $k$ . Mexican hat wavelets [20] are generated by the filter  $\varphi(s) := s^{1/2} \exp(-s^2)$  and in [8, 2] the filter map  $\varphi(s) := \exp(is)$ ,  $s \in [0, 2\pi]$ , defines the wave kernel signature. The spectral distances associated to this periodic filter identify local shape features by separating the contribution of different frequencies and of the corresponding eigenfunctions. Similarly to random walks [31], we introduce multi-scale kernels by integrating the moment of order  $k$  of the differential operator  $\Delta^\alpha \exp(-t\Delta^\alpha)$ . In this case, the filter map is  $\varphi(s) := t^k s^\alpha \exp(-ts^\alpha)$ , where  $k$  scales the rate of diffusion and  $\alpha$  controls the decay of the Laplacian eigenvalues to zero. The selection of the parameters  $\alpha$ ,  $k$  makes the multi-scale kernels more robust to geometric and topological noise; the integral over time also avoids the selection of the heat diffusion rate. Finally, the filter maps  $\varphi_t(s) := [\cos^{-1/2}(\sqrt{st}), s^{-1/4} \sin^{1/2}(\sqrt{st})]$  and  $\varphi(s, t) = \exp(s^r t)$  are associated to the diffusion equations  $(\partial_t^2 + \Delta) F(\cdot, t) = 0$  and  $(\partial_t + \Delta') F(\cdot, t) = 0$ , respectively.

Starting from these filters, we can design new distances; the only constraint is that  $\varphi$  is strictly positive and square integrable. In particular, the filter map has a compact support (e.g., periodic filter maps) or  $\lim_{s \rightarrow +\infty} \varphi(s) = 0$ . In this last case, the convergence of the filtered eigenvalues  $(\varphi(\lambda_i))_{i=1}^n$  to zero determines the capability of the spectral distances to locally or globally characterize the input shape, their smoothness and approximation accuracy through the truncated approximation (c.f., Eq. (5b)). Increasing the filter decay to zero, the effects of larger eigenvalues and of the corresponding eigenvectors on the filtered spectral distance are negligible with respect to the contribution of the lower eigenvalues. The resulting distance characterizes the global properties of the input shape, while poorly identifying its local properties. Reducing the filter decay to zero, local shape features are better characterized. Finally, a simple way to generate new kernels and distances is to compute a convex combination of filter maps. For instance (Fig. 2),

$\varphi^2$	Spect. dist.	$d^2(\mathbf{p}, \mathbf{q}) = \sum_{n=0}^{+\infty} \varphi^2(\lambda_n)  \phi_n(\mathbf{p}) - \phi_n(\mathbf{q}) ^2$	
		Associated equation	Kernel
$s^{-1}$	Comm.-time	$(\partial_t + \Delta^r) F(\cdot, t) = 0$	$\sum_{n=0}^{+\infty} t^k e^{-\lambda_n t}  \phi_n(\mathbf{p}) - \phi_n(\mathbf{q}) ^2$
$s^{-2}$	Biharm.	<i>Poly-harm. eq.</i>	
$s^{-k}$	Poly-harm.	<i>Poly-harm.</i>	
$e^{-st}$	Heat diff.	$(\partial_t + \Delta) F(\cdot, t) = 0$ <i>Heat diffusion eq.</i>	$\sum_{n=0}^{+\infty} e^{-\lambda_n t}  \phi_n(\mathbf{p}) - \phi_n(\mathbf{q}) ^2$
$e^{-ist}$	Wave ker.	$(\partial_t + i\Delta) F(\cdot, t) = 0$ <i>Schrodinger eq.</i>	$\sum_{n=0}^{+\infty} e^{-i\lambda_n t}  \phi_n(\mathbf{p}) - \phi_n(\mathbf{q}) ^2$

a trade-off between the measure of both local and global properties is achieved by selecting as  $\varphi$  a convex combination between the filters associated to the diffusion and biharmonic distances.

## 3. Spectrum-free computation

After introducing the discrete spectral distances (Sect. 3.1), we discuss their proposed spectrum-free computation, which is based on the Taylor approximation of the filter map (Sect. 3.2), and its specialization to the heat diffusion distances through the Padé-Chebyshev approximation (Sect. 3.3).

### 3.1. Discrete spectral distances

The spectral distances are discretized on the space of maps  $f: \mathcal{P} \rightarrow \mathbb{R}$ ,  $\mathbf{f} := (f(\mathbf{p}_i))_{i=1}^n$ , defined on the point set  $\mathcal{P} := \{\mathbf{p}_i\}_{i=1}^n$ . To this end (Sect. 4), we represent the Laplace-Beltrami operator on polygonal meshes and point sets in a unified way as  $\tilde{\mathbf{L}} := \mathbf{B}^{-1}\mathbf{L}$ , where  $\mathbf{B}$  is a positive definite matrix and  $\mathbf{L}$  is symmetric, positive semi-definite. Noting that  $B(i, j) = \langle \mathbf{1}_{\mathbf{p}_i}, \mathbf{1}_{\mathbf{p}_j} \rangle_2$ , where  $\mathbf{1}_{\mathbf{p}}$  is the map that takes value 1 at  $\mathbf{p}$  and 0 otherwise, the matrix  $\mathbf{B}$  discretizes the Borel measure  $\mu$  (Sect. 2.1) and  $\langle \mathbf{f}, \mathbf{g} \rangle_{\mathbf{B}} := \mathbf{f}^\top \mathbf{B} \mathbf{g}$  is the counterpart of the  $\mathcal{L}_2$  scalar product on the space of discrete maps on  $\mathcal{P}$ .

The couple  $(\tilde{\mathbf{L}}, \mathbf{B})$ , which defines the Laplacian matrix  $\tilde{\mathbf{L}}$ , is associated to the generalized eigensystem  $\mathbf{L}\mathbf{X} = \mathbf{B}\mathbf{X}\Lambda$ , with orthonormal eigenvectors  $\mathbf{X}^\top \mathbf{B} \mathbf{X} = \mathbf{I}$ . Noting that  $\varphi(\Lambda) = \text{diag}(\varphi(\lambda_i))_{i=1}^n$  and  $\tilde{\mathbf{L}} = \mathbf{X}\Lambda\mathbf{X}^\top \mathbf{B}$ , we get that  $\tilde{\mathbf{L}}^i = \mathbf{X}\Lambda^i \mathbf{X}^\top \mathbf{B}$  and the discretization of (1) is

$$\begin{aligned} \mathbf{K} &:= \varphi(\tilde{\mathbf{L}}) = \sum_{n=0}^{+\infty} \alpha_n (\mathbf{X}\Lambda\mathbf{X}^\top \mathbf{B})^n = \mathbf{X} \left( \sum_{n=0}^{+\infty} \alpha_n \Lambda^n \right) \mathbf{X}^\top \mathbf{B} \\ &= \mathbf{X}\varphi(\Lambda)\mathbf{X}^\top \mathbf{B}. \end{aligned}$$

Indeed, we approximate  $\Phi(f)$  as  $\mathbf{K}\mathbf{f} := \sum_{i=1}^n \varphi(\lambda_i) \langle \mathbf{f}, \mathbf{x}_i \rangle_{\mathbf{B}} \mathbf{x}_i$ .

From the eigenvectors' orthonormality, we get that

$$\begin{aligned} \mathbf{K}^\top \mathbf{B} \mathbf{K} &= \mathbf{B} \mathbf{X} \varphi^2(\Lambda) \mathbf{X}^\top \mathbf{B} \\ &= \mathbf{B} \tilde{\mathbf{K}}, \end{aligned} \quad (3)$$

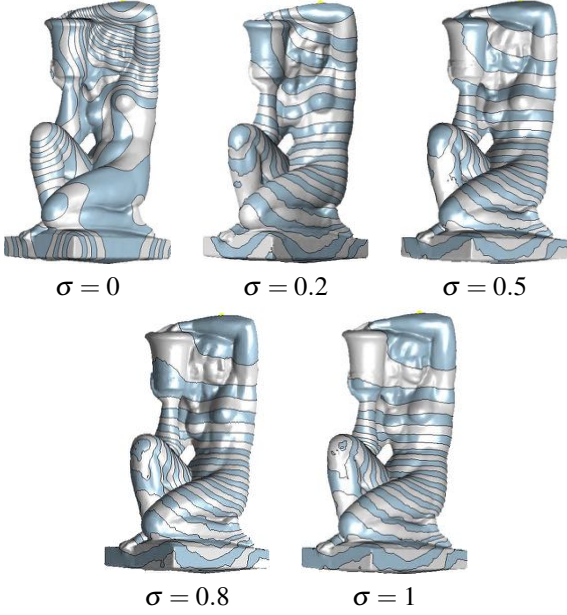


**Figure 2:** Level sets of the filtered spectral distance achieved as a convex combination of the filter maps associated to the diffusion ( $\sigma = 0$ ,  $t = 0.5$ ) and bi-harmonic ( $\sigma = 1$ ) distances.

where  $\tilde{\mathbf{K}} := \mathbf{X}\varphi^2(\Lambda)\mathbf{X}^\top\mathbf{B}$  is the spectral kernel associated to the filter  $\varphi^2$ . From Eq. (3), the discrete spectral distances are

$$\begin{aligned} d(\mathbf{p}_i, \mathbf{p}_j) &= \|\mathbf{K}(\mathbf{e}_i - \mathbf{e}_j)\|_{\mathbf{B}}^2 = (\mathbf{e}_i - \mathbf{e}_j)^\top \mathbf{K}^\top \mathbf{B} \mathbf{K} (\mathbf{e}_i - \mathbf{e}_j) \\ &= \sum_{l=1}^n \varphi^2(\lambda_l) |\langle \mathbf{x}_l, \mathbf{e}_i - \mathbf{e}_j \rangle_{\mathbf{B}}|^2. \end{aligned} \quad (4)$$

*Truncated approximation.* The computational limits for the evaluation of the whole spectrum of  $\tilde{\mathbf{L}}$ , which varies from  $O(n)$  to  $O(n^3)$  according to its sparsity, and the decay of the coefficients in Eq. (2b) are the main reasons behind the approximation of the solution to the spectral distances as a truncated sum; i.e.,

$$\begin{cases} \Phi_k \mathbf{f} = \sum_{i=1}^k \varphi(\lambda_i) \langle \mathbf{f}, \mathbf{x}_i \rangle_{\mathbf{B}} \mathbf{x}_i, & (a) \\ d^2(\mathbf{p}_i, \mathbf{p}_j) = \sum_{l=1}^k \varphi(\lambda_l) |\mathbf{x}_l^\top \mathbf{B} \mathbf{e}_i - \mathbf{x}_l^\top \mathbf{B} \mathbf{e}_j|^2, & (b) \end{cases} \quad (5)$$

where  $k$  is the number of selected eigenpairs. Even though the first  $k$  Laplacian eigenpairs are computed in super-linear time [35], the evaluation of the whole Laplacian spectrum is unfeasible for storage and computational cost, which are quadratic in the number of surface samples. In this case, the parameter  $k$  must be selected by the user and the approximation accuracy cannot be estimated without extracting the whole spectrum. Furthermore, the selection of filters that are periodic or do not decrease to zero highlights the need of defining a spectrum-free computation of the corresponding kernels and distances, which cannot be accurately approximated with the contribution of only a subpart of the Laplacian spectrum.

### 3.2. Spectrum-free computation of the spectral distances

A natural way to approximate a matrix function  $\varphi(\tilde{\mathbf{L}})$ ,  $\varphi: \mathbb{R}^+ \rightarrow \mathbb{R}$ , is through the truncated approximation of the Tay-

---

#### Algorithm 1 Evaluation of the spectral distance and kernel.

---

**Require:** A filter map  $\varphi: \mathbb{R} \rightarrow \mathbb{R}$ .

**Ensure:** The spectral distance  $d(\mathbf{p}_i, \mathbf{p}_j)$  in Eq. (4).

- 1: Compute the Taylor polynomial  $p_r(s) := \sum_{n=0}^r \alpha_n s^n$  of  $\varphi$  of degree  $r$ ,  $r \geq 1$ .
  - 2: Compute  $\mathbf{g}_1$  such that  $\mathbf{B}\mathbf{g}_1 = \mathbf{L}\mathbf{e}_i$
  - 3: **for**  $n = 1, \dots, r-1$  **do**
  - 4:   Compute  $\mathbf{g}_{n+1}$  such that  $\mathbf{B}\mathbf{g}_{n+1} = \mathbf{L}\mathbf{g}_n$
  - 5: **end for**
  - 6: Approximate  $\mathbf{K}\mathbf{e}_i$  as  $\alpha_0 \mathbf{e}_i + \sum_{n=1}^r \alpha_n \mathbf{g}_n$
  - 7: Repeat the previous steps for  $\mathbf{e}_j$
  - 8: Compute  $d(\mathbf{p}_i, \mathbf{p}_j) = \|\mathbf{K}\mathbf{e}_i - \mathbf{K}\mathbf{e}_j\|_{\mathbf{B}}$
  - 9: Compute  $K(\mathbf{p}_i, \mathbf{p}_j) = \mathbf{e}_i^\top \mathbf{K} \mathbf{e}_j$
- 

lor series of  $\varphi$ . More precisely [18], if  $\varphi(s) = \sum_{n=0}^{+\infty} \alpha_n s^n$  is the power series representation of  $\varphi$  on an open interval containing the spectrum of the matrix  $\tilde{\mathbf{L}}$  then  $\varphi(\tilde{\mathbf{L}}) = \sum_{n=0}^{+\infty} \alpha_n \tilde{\mathbf{L}}^n$ . An alternative is the Padé-Chebyshev approximation, which uses a rational polynomial and has been applied to the approximation of the heat diffusion kernel [27] (Sect. 3.3). To evaluate the spectral distance, we can proceed in two different ways, which are independent of the computation of the Laplacian spectrum and have the same approximation accuracy.

As first option, we approximate  $\mathbf{K}\mathbf{e}_i$  through the Taylor approximation  $\varphi(s) \approx p_r(s) := \sum_{n=0}^r \alpha_n s^n$  as

$$\mathbf{K}\mathbf{e}_i \approx \sum_{n=0}^r \alpha_n (\mathbf{B}^{-1}\mathbf{L})^n \mathbf{e}_i = \alpha_0 \mathbf{e}_i + \sum_{n=1}^r \alpha_n \mathbf{g}_n,$$

where  $\mathbf{g}_n$  satisfies the linear system  $\mathbf{B}\mathbf{g}_{n+1} = \mathbf{L}\mathbf{g}_n$ ,  $\mathbf{B}\mathbf{g}_1 = \mathbf{L}\mathbf{e}_i$ . Being the coefficient matrix  $\mathbf{B}$  sparse, symmetric, and positive definite, the vectors  $(\mathbf{g}_n)_{n=0}^r$  are computed in linear time by applying iterative solvers (e.g., conjugate gradient) or pre-factorizing  $\mathbf{B}$ . Then,  $d(\mathbf{p}_i, \mathbf{p}_j)$  is equal to the  $\mathbf{B}$ -norm of the vector  $(\mathbf{K}\mathbf{e}_i - \mathbf{K}\mathbf{e}_j)$ . Algorithm 1 summarizes the main step of the spectrum-free computation.

As second option, we rewrite the spectral distance (3) in terms of the kernel  $\tilde{\mathbf{K}}$  in Eq. (4) as

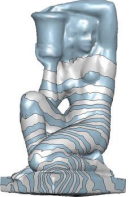
$$d(\mathbf{p}_i, \mathbf{p}_j) = \mathbf{e}_i^\top \tilde{\mathbf{K}} \mathbf{e}_i - 2\mathbf{e}_i^\top \tilde{\mathbf{K}} \mathbf{e}_j + \mathbf{e}_j^\top \tilde{\mathbf{K}} \mathbf{e}_j, \quad (6)$$

and  $d(\mathbf{p}_i, \mathbf{p}_j)$  is evaluated through the Taylor approximation of the new filter  $\varphi^2$ . Then,  $\tilde{\mathbf{K}}\mathbf{e}_i$ ,  $\tilde{\mathbf{K}}\mathbf{e}_j$  are computed through the Taylor approximation and the resulting vectors are then multiplied by  $\mathbf{e}_i^\top \tilde{\mathbf{B}}$ ,  $\mathbf{e}_j^\top \tilde{\mathbf{B}}$ , without extracting the Laplacian spectrum.

From the upper bound

$$\begin{aligned} \left\| \varphi(\tilde{\mathbf{L}}) - \sum_{n=0}^r \alpha_n \tilde{\mathbf{L}}^n \right\|_2 &\leq \frac{n}{(r+1)!} \left\| \tilde{\mathbf{L}}^{r+1} \varphi^{(r+1)}(\tilde{\mathbf{L}}) \right\|_2 \\ &\leq \frac{n}{(r+1)!} \|\tilde{\mathbf{L}}\|_2^{r+1} \|\varphi^{(r+1)}(\tilde{\mathbf{L}})\|_2 \\ &\leq \frac{n}{(r+1)!} \left[ \frac{\lambda_{\max}(\tilde{\mathbf{L}})}{\lambda_{\min}(\tilde{\mathbf{B}})} \right]^{r+1} \|\varphi^{(r+1)}(\tilde{\mathbf{L}})\|_2, \end{aligned}$$

it follows that the approximation accuracy is mainly controlled by the degree of the Taylor approximation and the variation

Low-resolution shape: biharmonic distances			
FEM		Voronoi-cot	
			
$k = 10$	$k = 500$	$k = 10$	$k = 500$
High-resolution shape: biharmonic distances			
FEM		Voronoi-cot	
			
$k = 10$	$k = 500$	$k = 10$	$k = 500$

**Figure 3:** Biharmonic distance on a surface at different resolutions, with different Laplacian weights and  $k$  eigenpairs.

of the ratio between the maximum eigenvalue of  $\mathbf{L}$  and the minimum eigenvalue of  $\mathbf{B}$ . If necessary, a higher approximation accuracy is achieved by slightly increasing the degree  $r$ . Finally, the proposed computation of both the spectral kernel and distance is independent of the discretization of the input surface as a polygonal mesh or a point cloud. In case of a complex kernel, it is enough to apply the previous discussion to its real and imaginary parts; e.g., for the wave kernel we consider the series  $\sin(\tilde{\mathbf{L}}) = \sum_{n=0}^{+\infty} (-1)^n \tilde{\mathbf{L}}^{2n+1} / (2n+1)!$  and  $\cos(\tilde{\mathbf{L}}) = \sum_{n=0}^{+\infty} (-1)^n \tilde{\mathbf{L}}^{2n} / (2n)!$ .

In previous work, the spectral distances are discretized with respect to the Euclidean scalar product as

$$d^2(\mathbf{p}_i, \mathbf{p}_j) = \sum_{l=1}^n \varphi(\lambda_l) |\mathbf{x}_l^\top \mathbf{e}_i - \mathbf{x}_l^\top \mathbf{e}_j|^2 \quad (7)$$

$$= \mathbf{e}_i^\top \mathbf{K}^* \mathbf{e}_i - 2\mathbf{e}_i^\top \mathbf{K}^* \mathbf{e}_j + \mathbf{e}_j^\top \mathbf{K}^* \mathbf{e}_j,$$

where  $\mathbf{K}^* := \mathbf{X}\varphi(\Lambda)\mathbf{X}^\top$  is the corresponding kernel. Comparing the proposed discretization of the spectral distance with previous work, we get that (6) is achieved from (7) by replacing  $x_k(\mathbf{p}_i) = \mathbf{e}_i^\top \mathbf{x}_k$  with  $\mathbf{e}_i^\top \mathbf{B}\mathbf{x}_k$ . However, Eq. (7) does not take into account the intrinsic  $\mathbf{B}$ -scalar product, thus disregarding the geometry of the input data and the underlying generalized eigenproblem.

### 3.3. Spectrum-free computation of the diffusion distances

We now specialize the previous approach to the spectrum-free computation of the heat diffusion distances. To this end [27], we recall that the heat diffusion kernel is defined in terms of the Laplacian eigensystem  $(\mathbf{X}, \Lambda)$  as  $\mathbf{K}_t = \mathbf{X}\varphi(\Lambda)\mathbf{X}^\top \mathbf{B}$ , where  $\varphi(\Lambda) := \exp(-t\Lambda)$  is the diagonal matrix achieved by exponentiating the Laplacian eigenvalues with respect to time.

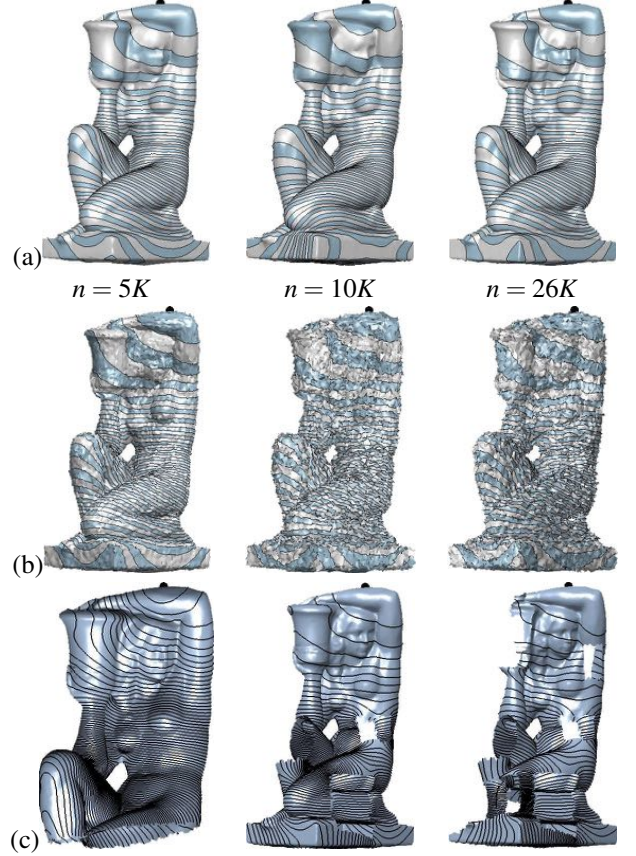


**Figure 4:** Stability of the biharmonic distance from a source (black) point with respect to (a) sampling, (b) noise, (c) holes.

Rewriting the Laplacian matrix as  $\tilde{\mathbf{L}} = \mathbf{X}\Lambda\mathbf{X}^\top \mathbf{B}$ , we get that  $\tilde{\mathbf{L}}^n = \mathbf{X}\Lambda^n \mathbf{X}^\top \mathbf{B}$  and

$$\exp(-t\tilde{\mathbf{L}}) := \sum_{n=0}^{+\infty} \frac{(-t\tilde{\mathbf{L}})^n}{n!} = \mathbf{X} \sum_{n=0}^{+\infty} \frac{(-\Lambda t)^n}{n!} \mathbf{X}^\top \mathbf{B}$$

$$= \mathbf{X} \exp(-\Lambda t) \mathbf{X}^\top \mathbf{B} = \mathbf{K}_t;$$

i.e., the weighted diffusion kernel  $\mathbf{K}_t$  is still the exponential of the Laplacian matrix  $\tilde{\mathbf{L}}$ . Then, we can apply the rational Padé-Chebyshev approximation, which is based on the extension of the minmax Padé-Chebyshev theory to rational fractions [18] (Ch. 11). More precisely, we compute the  $(r, r)$ -degree rational function  $c_{rr}(s)$  that provides the best approximation of the exponential function with respect to the  $\mathcal{L}^\infty(\mathbb{R}^+)$  norm. Using algebraic rules, this solution is  $c_{rr}(s) = \alpha_0 + \sum_{i=1}^r \alpha_i / (s - \theta_i)$  and the exponential matrix is approximated by  $\exp(\mathbf{C}) \approx \alpha_0 \mathbf{I} + \sum_{i=1}^r \alpha_i (\mathbf{C} - \theta_i \mathbf{I})^{-1}$ . In this representation, the poles  $\{\theta_i\}_{i=1}^r$  and the coefficients  $\{\alpha_i\}_{i=1}^r$  have been computed for  $r := 5, 7$  [16]. Applying the approximation

$$\mathbf{F}(t) = \exp(-t\tilde{\mathbf{L}})\mathbf{f} \approx - \sum_{i=1}^r \alpha_i (\tilde{\mathbf{L}} + \theta_i \mathbf{I})^{-1} \mathbf{f}, \quad r = 7, \quad (8)$$

the vector  $\mathbf{F}(t) = \sum_{i=1}^r \mathbf{g}_i$  is computed as the sum of the solutions of  $r$  sparse linear systems  $(t\tilde{\mathbf{L}} + \theta_i \mathbf{I})\mathbf{g}_i = \alpha_i \mathbf{f}$ ,  $i = 1, \dots, r$ . In this way, we avoid the computation of the spectrum of  $\tilde{\mathbf{L}}$ .

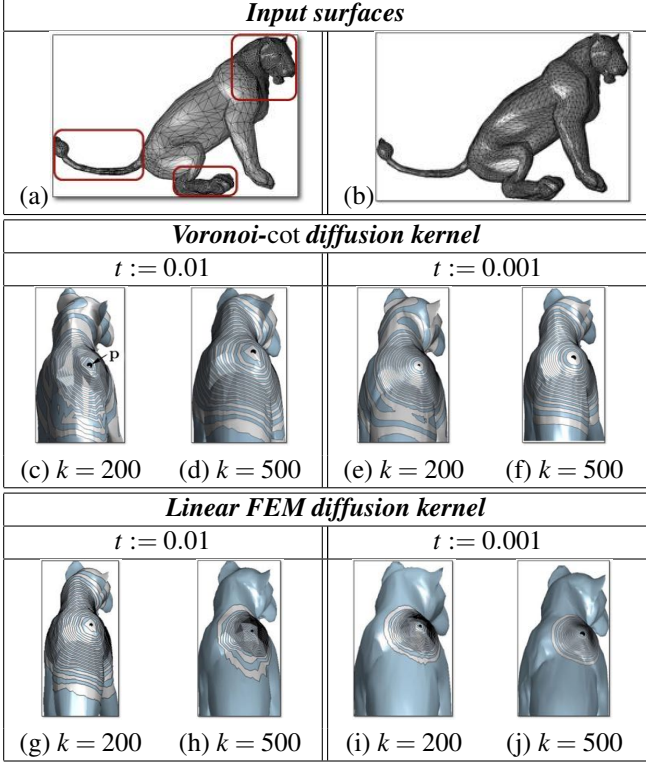


**Figure 5:** Approximation (c.f., Eq. (5a)) of the diffusion map  $\mathbf{K}_t \mathbf{e}_i$  using  $k$  Laplacian eigenpairs, with (c-f) Voronoi-cot and (g-j) FEM weights on a (a) coarse and (b) fine surface sampling.

According to [36], the  $\ell_2$  approximation error between  $\exp(-t\mathbf{C})$  and its rational approximation  $c_{rr}(t\mathbf{C})$ ,  $\mathbf{C} := \tilde{\mathbf{L}}$ , is lower than the uniform rational Chebyshev constant  $\sigma_{rr}$ . Since this constant is known, independent of  $t$ , and related to the degree of the rational Padé-Chebyshev approximation by the relation  $\sigma_{rr} \approx 10^{-r}$ ,  $r := 7$  provides an approximation error that is satisfactory for the approximation of  $\mathbf{K}_t \mathbf{f}$ . For a general degree  $r$  and a fixed value of  $t$ , the coefficients of the rational approximation of the exponential map, are computed using the Padé method [18].

*Computation of the heat diffusion distances.* According to [11] and Eq. (4), let us introduce the *diffusion distance*, with respect to  $\mathbf{K}_t$  and  $\langle \cdot, \cdot \rangle_{\mathbf{B}}$ , as

$$d_t^2(\mathbf{p}_i, \mathbf{p}_j) = (\mathbf{e}_i - \mathbf{e}_j)^\top \mathbf{K}_t^\top \mathbf{B} \mathbf{K}_t (\mathbf{e}_i - \mathbf{e}_j), \quad (9)$$

$$= \sum_{l=1}^n \exp(-2\lambda_l t) |\langle \mathbf{x}_l, \mathbf{e}_i - \mathbf{e}_j \rangle_{\mathbf{B}}|^2,$$

where we have used the identity  $\mathbf{K}_t^\top \mathbf{B} \mathbf{K}_t = \mathbf{B} \mathbf{X} \mathbf{D}_{2t} \mathbf{X}^\top \mathbf{B}$  in the last equation. Noting that  $\mathbf{K}_t^\top \mathbf{B} \mathbf{K}_t = \mathbf{B} \mathbf{K}_{2t}$  and applying Eq. (9), the distance is expressed in terms of the kernel  $\mathbf{H}_t := \mathbf{B} \mathbf{K}_{2t}$  as

$$d_t^2(\mathbf{p}_i, \mathbf{p}_j) = \mathbf{e}_i^\top \mathbf{B} \mathbf{K}_{2t} \mathbf{e}_i - 2\mathbf{e}_i^\top \mathbf{B} \mathbf{K}_{2t} \mathbf{e}_j + \mathbf{e}_j^\top \mathbf{B} \mathbf{K}_{2t} \mathbf{e}_j.$$

Then,  $\mathbf{K}_{2t} \mathbf{e}_i$ ,  $\mathbf{K}_{2t} \mathbf{e}_j$  are computed through the Padé-Chebyshev approximation and the resulting vectors are then multiplied by  $\mathbf{e}_i^\top \mathbf{B}$ ,  $\mathbf{e}_j^\top \mathbf{B}$ , without extracting the Laplacian spectrum.

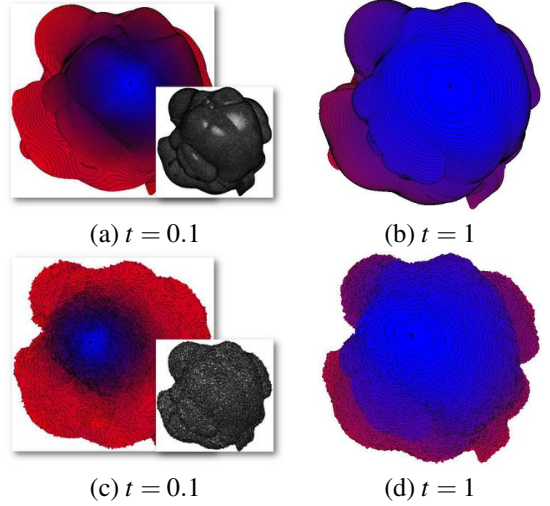


**Figure 6:** Level sets of the linear FEM diffusion distance (9), computed using the Padé-Chebyshev approximation ( $r := 7$ ) in Eq. (8), from a source point (black dot), with different values of  $t$ , on a (a,b) smooth and (c,d) noisy surface.

#### 4. Results and discussion

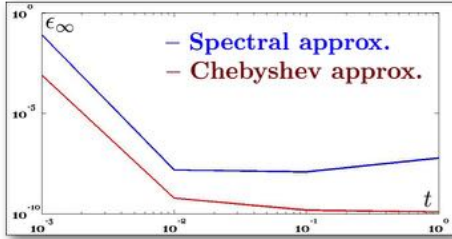
Firstly, we detail how to represent the Laplace-Beltrami operator on polygonal meshes and point sets in a unified way. Then, we discuss the main features of the proposed approach in terms of smoothness, stability to shape discretization, approximation accuracy, and computational cost.

*Laplacian matrix on meshes and point sets.* Assuming that the input shape  $\mathcal{M}$  is discretized as a polygonal mesh or a point set, we represent the Laplacian matrix as  $\tilde{\mathbf{L}} := \mathbf{B}^{-1} \mathbf{L}$ , where  $\mathbf{L}$  is a symmetric, positive semi-definite matrix and  $\mathbf{B}$  is a symmetric and positive definite matrix. On triangle meshes,  $\mathbf{L}$  is the Laplacian matrix with cotangent weights and  $\mathbf{B}$  is the diagonal matrix whose entries are the areas of the Voronoi regions of the mesh vertices (*Voronoi-cot weights*) [14]. Alternatively,  $\mathbf{B}$  is the FEM mass matrix (*linear FEM weights*) [32, 35], which encodes the variation of the triangle areas. If  $\mathbf{B} := \mathbf{I}$ , then we get the Laplacian matrix with cot weights [30]. On polygonal meshes, we consider the Laplacian discretization proposed in [1], which provides a generalization of the Laplacian matrix with cot-weights to surface meshes with non-planar, non-convex faces. On point sets [23],  $\mathbf{L}$  is the Laplacian matrix associated to the Gaussian kernel and the diagonal matrix  $\mathbf{B}$  encodes the area of the Voronoi cells. This discretization and its previous version [4, 5] ( $\mathbf{B} := \mathbf{I}$ ) converge to the Laplace-Beltrami operator of the underlying manifold, as the sampling density increases and  $t$  tends to zero.

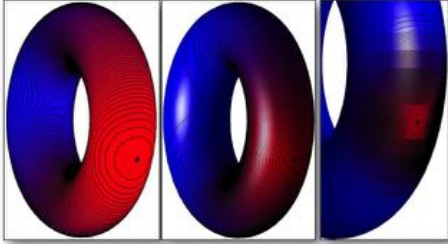
*Biharmonic distances.* In Fig. 3, the approximation of the biharmonic kernel with a subset of the Laplacian spectrum (Eq. (5b)) presents local artifacts, which are represented by isolated level sets and are due to the use of only a part of the Laplacian spectrum. While these artifacts are reduced by increasing the number of eigenpairs without disappearing, the spectrum-free



**Figure 7:** Level sets of the linear FEM diffusion distances (9), computed using the Padé-Chebyshev method ( $r := 7$ ), from a source point (black dot) on partially-sampled surfaces. The behavior of the level sets remains almost unchanged and coherent with respect to the original shape (left).



(a)



(b)

**Figure 8:** (a)  $\ell_\infty$  error  $\epsilon_\infty$  (y-axis) between the ground-truth diffusion distances and its approximation with (blue line)  $k = 500$  Laplacian eigenpairs (red line) and the Padé-Chebyshev approximation ( $r := 7$ ), with different values of  $t$  (x-axis). (b) Level sets of the diffusion distance from a source point (black dot) with different values of  $t$ .

approach does not have this behavior. In Fig. 4, the smooth and uniform distribution of the level sets of the biharmonic distance around the anchor point (black dot) confirms the stability of the proposed computation with respect to surface sampling, noise, and missing parts.

*Heat diffusion and wave kernel distances.* We now consider the solution  $\mathbf{K}_t \mathbf{e}_i$  to the heat diffusion process, whose initial condition takes value 1 at the anchor point  $\mathbf{p}_i$  and 0 otherwise. On irregularly sampled data, the linear FEM heat kernel (Fig. 5) provides smooth level sets that are well-distributed around the anchor point  $\mathbf{p}_i$ ; on the contrary, the Voronoi-cot heat kernel is more sensitive to the surface sampling. On noisy (Fig. 6) and partially-sampled data (Fig. 7), the analogous behavior of the level sets and color maps also confirms the robustness of the linear FEM heat distances. Fig. 8 shows the  $\ell_\infty$  approximation error between the ground-truth heat diffusion distances from a source point and its approximation with  $k = 500$  Laplacian eigenpairs and the Padé-Chebyshev approximation. While

the approximation error of the diffusion distance with the same number of Laplacian eigenpairs decreases and becomes more sensible to local noise as  $t$  diminishes, the Padé-Chebyshev approximation provides a lower approximation error for any  $t$ .

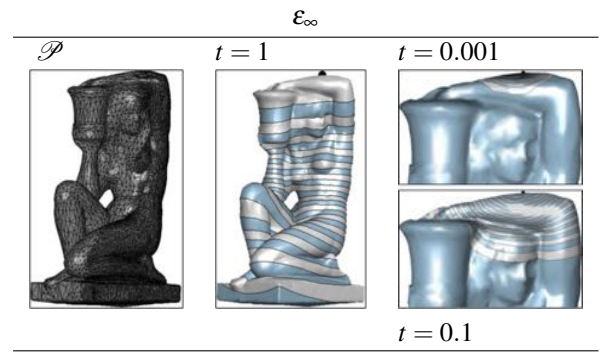
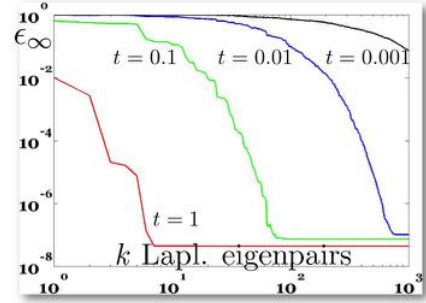


**Figure 9:**  $\ell_\infty$  error (y-axis)  $\epsilon_\infty := \|\mathbf{K}_t \mathbf{f} - \mathbf{F}_k(t)\|_\infty$  between the Padé-Chebyshev approximation ( $r := 7$ ) of  $\mathbf{F}(t) = \mathbf{K}_t \mathbf{e}_i$  and the partial spectral representation  $\mathbf{F}_k(t)$  in Eq. (5a), computed on an irregularly sampled shape, with respect to a different number  $k$  (x-axis,  $k \leq 10^3$ ) of eigenpairs and values of  $t$ .

We have further analyzed the different accuracy (Fig. 9) of the spectral and Padé-Chebyshev approximation of the heat kernel by measuring the  $\ell_\infty$  approximation error (y-axis) between the spectral representation of the heat kernel  $\mathbf{K}_t$ , computed using a different number  $k$  (x-axis) of eigenfunctions, and the corresponding Padé-Chebyshev approximation. For small values of  $t$ , the partial spectral representation requires a large number  $k$  of Laplacian eigenvectors to recover local details. For instance (Fig. 9), selecting  $1K$  eigenpairs the approximation error remains higher than  $10^{-2}$ ; in fact, local shape features encoded by  $\mathbf{K}_t$  for a small  $t$  are recovered using the eigenvectors associated with high frequencies, thus requiring the computation of a large part of the Laplacian spectrum. For large values of  $t$ , increasing  $k$  strongly reduces the approximation error until it becomes almost constant and close to zero. In this case, the behavior of the heat kernel is mainly influenced by the Laplacian eigenvectors related to the eigenvalues of smaller magnitude. We conclude that the spectral representation generally requires a high number of eigenpairs without achieving an accuracy of the same order of the spectrum-free approximation through the Padé-Chebyshev method. The proposed approach guarantees the smoothness of the heat diffusion distance at small and large scales and it is not affected by the irregular surface sampling.

The value of  $t$  influences the conditioning number of the matrices  $(t\mathbf{L} + \theta_i \mathbf{B})$ ,  $i = 1, \dots, r$ . Our experiments (Fig. 10) have

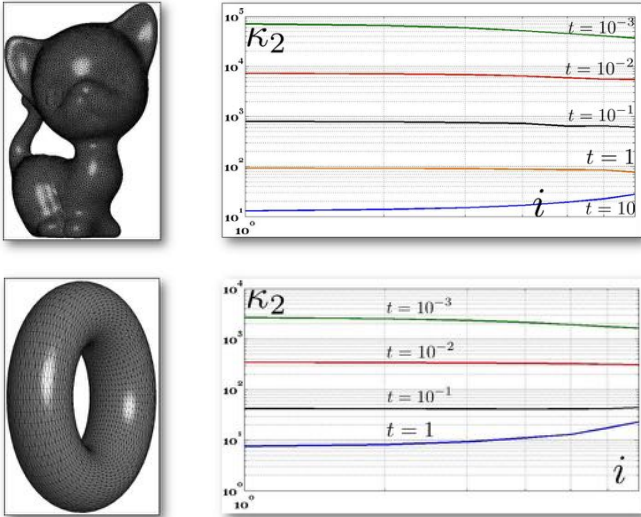


**Figure 10:** Conditioning number  $\kappa_2$  (y-axis) of the matrices  $\{(t\mathbf{L} + \theta_i\mathbf{B})\}_{i=1}^7$ , for several values the time parameter  $t$ ; the indices of the coefficients  $\{\theta_i\}_{i=1}^7$  are reported on the x-axis.

shown that the linear systems in Eq. (8) are generally well-conditioned; in any case, pre-conditioners and regularization techniques [18] can be applied to attenuate numerical instabilities. Since our approach works mainly on matrices, the computation of the heat diffusion distance and kernel is independent of the discretization of the input surface as a manifold/non-manifold polygonal [1] mesh or a point cloud.

The spectrum-free computation on point-sampled surfaces or non-manifold meshes (Fig. 11) is one of the novelties of the proposed approach with respect to previous work, which uses multi-resolutive and prolongation operators [37] on manifold triangle meshes. Timings (Table 1, Fig. 12) are reduced from 20 up to 1200 times with respect to the approximation based on a fixed number of Laplacian eigenpairs. Laplacian eigenvectors have been computed with the Arnoldi iteration method [22, 34].

## 5. Conclusions and future work

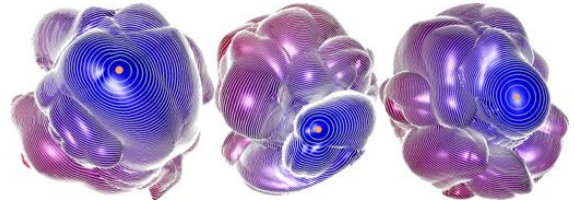
This paper has presented a novel definition and efficient computation of Laplacian spectral distances and kernels through the solution of a set of sparse, symmetric, well-conditioned linear systems and a sequence of matrix-vector multiplications. With respect to previous work, we provide an efficient computation of spectral distances and kernel on polygonal and point-sampled surfaces, thus avoiding the computation of the Laplacian spectrum, the selection of a specific subset of eigenpairs, and the use of multiresolutive prolongation operators. Since our approach works mainly on matrices, the computation of the spectral distances and kernels is independent of the discretization of the input surface as a manifold/non-manifold polygonal mesh or a point cloud. For point-sampled surfaces, we simply apply the spectrum-free computation to the corresponding Laplacian matrix. The spectrum-free computation



(a) Heat diffusion distances



(b) Heat diffusion distances



(c) Bi-harmonic distances

**Figure 11:** Spectrum-free computation of distances from a source point (orange) on (a) locally non-manifold, (b) a bordered (bottom), and (c) point-sampled surface. In (c), the spectral distance has been computed on a point sets with 150K samples and rendered on the underlying triangle mesh. For the computation of the diffusion distance, we have used the Padé-Chebyshev approximation of order  $r := 7$ .

of Laplacian distances and kernels on point-sampled surfaces or non-manifold meshes is one of the novelties of the proposed approach with respect to previous work, which uses multi-resolutive and prolongation operators on manifold triangle meshes. As future work, we foresee the analysis of the main constraints that the filter map should satisfy in order to define new Laplacian spectral distances and kernels. Another interesting direction is the study of the limit properties of the proposed computation on point-sampled surfaces.

**Acknowledgements.** Special thanks are given to the anonymous Reviewers for their valuable comments. This work has been partially supported by the Project “Methods and Techniques for the Development of Innovative Systems for Modeling and Analyzing Biomedical Data for Supporting Assisted Diagnosis”, PO CRO Programme, European Social Funding Scheme, Regione Liguria, and the FP7 Integrated Project IQMULUS - “A High Volume Fusion and Analysis Platform for Geospatial Point Clouds, Coverages, and Volumetric Data Sets”. 3D shapes are courtesy of the AIM@SHAPE Repository.

- [1] M. Alexa and M. Wardetzky. Discrete laplacians on general polygonal meshes. *ACM Transactions on Graphics*, 30(4), 2011.
- [2] M. Aubry, U. Schlickewei, and D. Cremers. The wave kernel signature:

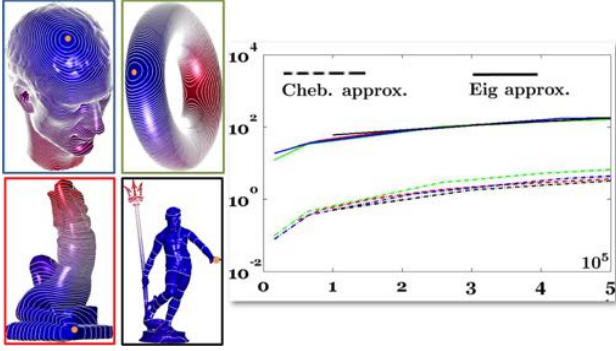


**Figure 12:** Computational cost (in seconds, y-axis, log-scale) for the evaluation of the diffusion distances on 3D shapes with  $n$  samples (x-axis), approximated with (straight line)  $k = 500$  eigenpairs and (dotted line) the Padé-Chebyshev approximation. Colors from the source (orange) point vary from blue (null distance) to red (maximum distance). Timings are reported in Table 1.

**Table 1:** Timings (in seconds, Fig. 12(c)) for the evaluation of the heat diffusion kernels on 3D shapes with  $n$  points, approximated with  $k = 500$  eigenpairs (Eigs) and the Padé-Chebyshev approximation (Cheb.). Column '×' indicates the number of times the computational cost is reduced. Tests have been performed on a 2.7 GHz Intel Core i7 Processor, with 8 GB memory.

Acquarius Fig. 12				Neptune Fig. 12(b)			
$n$	Eigs	Cheb.	×	$n$	Eigs	Cheb.	×
5K	30.06	0.26	115	10K	59.65	0.50	119
25K	97.25	1.83	53	30K	111.28	1.78	62
35K	130.39	2.61	49	50K	176.47	3.21	54
50K	173.78	3.60	48	100K	372.16	7.44	50

Torus Fig. 12(c)				Julius Fig. 12(d)			
$n$	Eigs	Cheb.	×	$n$	Eigs	Cheb.	×
2K	12.00	0.01	1200	2K	18.47	0.08	230
6K	33.28	0.45	73	7K	35.89	0.37	97
26K	100.88	2.89	34	22K	82.47	1.42	58
49K	140.00	5.14	33	43K	173.52	3.71	46
58K	186.06	7.92	23	50K	174.89	4.34	40

A quantum mechanical approach to shape analysis. In *IEEE International Conference on Computer Vision Workshops*, pages 1626–1633, 2011.

[3] M. Belkin and P. Niyogi. Laplacian eigenmaps for dimensionality reduction and data representation. *Neural Computations*, 15(6):1373–1396, 2003.

[4] M. Belkin and P. Niyogi. Convergence of Laplacian eigenmaps. In *NIPS*, pages 129–136, 2006.

[5] M. Belkin and P. Niyogi. Towards a theoretical foundation for Laplacian-based manifold methods. *Journal of Computer System Sciences*, 74(8):1289–1308, 2008.

[6] A. Bronstein, M. Bronstein, R. Kimmel, M. Mahmoudi, and G. Sapiro. A Gromov-Hausdorff framework with diffusion geometry for topologically-robust non-rigid shape matching. *International Journal of Computer Vision*, 2-3:266–286, 2010.

[7] A. M. Bronstein, M. M. Bronstein, M. Ovsjanikov, and L. J. Guibas. Shape Google: geometric words and expressions for invariant shape retrieval. *ACM Transactions on Graphics*, 30(1), 2011.

[8] M.M. Bronstein and A.M. Bronstein. Shape recognition with spectral distances. *IEEE Transactions on Pattern Analysis and Machine Intelligence*, 33(5):1065–1071, 2011.

[9] M.M. Bronstein and I. Kokkinos. Scale-invariant heat kernel signatures for non-rigid shape recognition. In *IEEE Conference on Computer Vision and Pattern Recognition*, pages 1704–1711, 2010.

[10] W. J. Cody, G. Meinardus, and R. S. Varga. Chebyshev rational approximations to  $\exp(-z)$  in  $(0, +\infty)$  and applications to heat-conduction prob-

lems. *Journal of Approximation Theory*, 2:50–65, 1969.

[11] R. R. Coifman and S. Lafon. Diffusion maps. *Applied and Computational Harmonic Analysis*, 21(1):5–30, 2006.

[12] K. Crane, C. Weischedel, and M. Wardetzky. Geodesics in Heat: A New Approach to Computing Distance Based on Heat Flow. *ACM Transactions on Graphics*, 2013.

[13] F. de Goes, S. Goldenstein, and L. Velho. A hierarchical segmentation of articulated bodies. *Computer Graphics Forum*, 27(5):1349–1356, 2008.

[14] M. Desbrun, M. Meyer, P. Schröder, and A. H. Barr. Implicit fairing of irregular meshes using diffusion and curvature flow. In *ACM Siggraph*, pages 317–324, 1999.

[15] T. K. Dey, P. Ranjan, and Y. Wang. Convergence, stability, and discrete approximation of laplace spectra. *ACM Symposium Discrete Algorithms*, pages 650–663, 2010.

[16] E. Gallopoulos and Y. Saad. Efficient solution of parabolic equations by Krylov approximation methods. *SIAM Journal of Scientific Statistical Computation*, 13:1236–1264, 1992.

[17] K. Gebal, J. A. Bærentzen, H. Aanæs, and R. Larsen. Shape analysis using the auto diffusion function. *Computer Graphics Forum*, 28(5):1405–1413, 2009.

[18] G. Golub and G.F. VanLoan. *Matrix Computations*. John Hopkins University Press, 2nd Edition, 1989.

[19] D. K. Hammond, P. Vandergheynst, and R. Gribonval. Wavelets on graphs via spectral graph theory. *Applied and Computational Harmonic Analysis*, 30(2):129–150, 2011.

[20] T. Hou and H. Qin. Continuous and discrete mexican hat wavelet transforms on manifolds. *Graphical Models*, 74(4):221–232, 2012.

[21] S. Lafon, Y. Keller, and R. R. Coifman. Data fusion and multicue data matching by diffusion maps. *IEEE Transactions on Pattern Analysis Machine Intelligence*, 28(11):1784–1797, 2006.

[22] R.B. Lehoucq and D. C. Sorensen. Deflation techniques for an implicitly re-started Arnoldi iteration. *SIAM Journal of Matrix Analysis and Applications*, 17:789–821, 1996.

[23] Y. Liu, B. Prabhakaran, and X. Guo. Point-based manifold harmonics. *IEEE Transactions on Visualization and Computer Graphics*, 18(10):1693–1703, 2012.

[24] C. Moler and C. Van Loan. Nineteen dubious ways to compute the exponential of a matrix, twenty-five years later. *SIAM Review*, 45(1):3–49, 2003.

[25] M. Ovsjanikov, M. Ben-Chen, J. Solomon, A. Butscher, and L. J. Guibas. Functional maps: a flexible representation of maps between shapes. *ACM Transactions on Graphics*, 31(4):30, 2012.

[26] M. Ovsjanikov, Q. Mérigot, F. Méholi, and L. Guibas. One point isometric matching with the heat kernel. *ACM Symposium on Discrete Algorithms*, pages 650–663, 2010.

[27] G. Patanè. wFEM heat kernel: Discretization and applications to shape analysis and retrieval. *Computer Aided Geometric Design*, 2013.

[28] G. Patanè and M. Spagnuolo. Heat diffusion kernel and distance on surface meshes and point sets. *Computers & Graphics*, 37(6):676–686, 2013.

[29] G. Patanè and M. Spagnuolo. An interactive analysis of harmonic and diffusion equations on discrete 3D shapes. *Computer & Graphics*, 2013.

[30] U. Pinkall and K. Polthier. Computing discrete minimal surfaces and their conjugates. *Experimental Mathematics*, 2(1):15–36, 1993.

[31] K. Ramani and A. Sinha. Multiscale kernels using random walks. *Computer Graphics Forum*, 2013.

[32] M. Reuter, F.-E. Wolter, and N. Peinecke. Laplace-Beltrami spectra as Shape-DNA of surfaces and solids. *Computer-Aided Design*, 38(4):342–366, 2006.

[33] R. M. Rustamov. Multiscale biharmonic kernels. *Computer Graphics Forum*, 30(5):1521–1531, 2011.

[34] D. C. Sorensen. Implicit application of polynomial filters in a k-step Arnoldi method. *SIAM Journal of Matrix Analysis and Applications*, 13(1):357–385, January 1992.

[35] B. Vallet and B. Lévy. Spectral geometry processing with manifold harmonics. *Computer Graphics Forum*, 27(2):251–260, 2008.

[36] R.S. Varga. *Scientific computation on mathematical problems and conjectures*. SIAM, CBMS-NSF regional conference series in applied mathematics, 1990.

[37] A. Vaxman, M. Ben-Chen, and C. Gotsman. A multi-resolution approach to heat kernels on discrete surfaces. *ACM Transactions on Graphics*,

29(4):1–10, 2010.

- [38] Y. Wang. Approximating gradients for meshes and point clouds via diffusion metric. *Computer Graphics Forum*, 28:1497–1508(12), 2009.
- [39] B. Xiaoa, E. R. Hancock, and R.C. Wilsonb. Geometric characterization and clustering of graphs using heat kernel embeddings. *Image and Vision Computing*, 28(6):1003 – 1021, 2010.